Model Identification and $\mathcal{H}_\infty$ Attitude Control for Quadrotor MAV's

Ole Falkenberg[1], Jonas Witt[1], Ulf Pilz[2], Uwe Weltin[1] and Herbert Werner[2]

[1] Hamburg University of Technology, Institute for Reliability Engineering, Eißendorfer Str. 40, 21073 Hamburg, Germany
[2] Hamburg University of Technology, Institute of Control Systems, Eißendorfer Str. 40, 21073 Hamburg, Germany
{ole.falkenberg,jonas.witt,ulf.pilz,weltin,h.werner}@tu-harburg.de

Abstract This paper presents the results of modelling, parameter identification and control of the rotational axes of a quadrotor robot. The modelling is done in Newton-Euler Formalism and has been published before. Contrarily, our method uses a Grey-Box-based, iterative parameter identification approach, the results of which can easily be reproduced and offers great accuracy. By neglecting nonlinear and cross-coupling effects, only three to four parameters have to be identified per axis, depending on the order of the motor dynamics. Based on the achieved results we were able to design an aggressive $\mathcal{H}_\infty$ attitude controller, which shows superior performance to the normal PID-like controllers. With an anti-windup compensator based on Riccati–equations we are able to show exceptional input disturbance rejection, even with disturbances saturating the engines.

Keywords: micro unmanned aerial vehicle (MAV), robust control, system identification, quadrotor

1 Introduction

Quadrotor robots are a popular research platform e.g. for autonomous navigation or multi-agent-control. Famous projects are located in the GRASP-laboratory at the University of Pennsylvania [1], the Flying Machine Area at the ETH Zürich [2] or the STARMAC II–project at the University of Stanford [3]. These projects rely on commercial quadrotors, except for the latter. The Hamburg University of Technology has developed an own quadrotor platform for research purposes, which shows exceptional research capabilities because of its insight to the lowest levels of interest. These insights reveal the drawbacks of common quadrotor controller designs. Especially the non–ideal performance of the common onboard MEMS–sensors in position estimation has driven many projects to use external camera systems, which provide great accuracy for the estimation of the quadrotors states, but also limits the operational area to the laboratory. Unlike those projects we do not rely on external camera systems, but only onboard sensors, onboard camera–vision and GPS, see [4]. Our research interest cover vision–based

navigation, formation control and aggressive manoevering. This paper focuses on linear parameter identification and attitude control, though. Attitude control is the most inner control loop and is crucial for a good overall flight performance. Therefore an advanced controller design scheme like $\mathcal{H}_\infty$-loopshaping should be favoured over traditional PID-control.

Beside the choice of a controller design scheme, an accurate model of the dynamics to be controlled is another crucial aspect for controller performance. The quadrotors physical equations of motion are well known and were published in e.g. [5] or [6]. But only few has been published about actual parameter identification based on real experiments. The reason for this absence is the unstable system dynamics of the quadrotor, which makes open-loop identification non-practical. Additionally, a bad signal to noise ratio and cross-coupling effects make for a challenging setup. The noise sources are mainly vibration and sensor noise.

Some first-order studies on aerodynamics have been done in [7] which have been extended in [3]. Infact, aerodynamics can have a major influence on attitude control. Especially the nonlinear variation of the induced velocity ν_i in forward flight, which effectively changes the relation of power P and thrust T, can lead to undesired behaviour. In [3], blade flapping is specified as another major source of nonlinearity causing undesired forces and torques. In this paper we present an advanced attitude control scheme, which is based on a linearized model, feasible in most common flight situations. Though its validity is limited:

- Nonlinearities caused by aerodynamics increase during forward flight with relative movement speed.
- During fast descent the quadrotor can enter the so-called vortex-ring-state, which cannot be estimated with normal momentum theory.
- The so-called Ground Effect augments thrust, if the quadrotor operates close to the ground ($\approx$ one rotor radius, see [5]).

However, it is obvious that a linear approach has advantages due to very powerful controller design and analysis tools. Using the linearized system dynamics we show that each quadrotor axis can be identified separately with a Grey-Boxed-based identification. With that model we have designed an aggressive $\mathcal{H}_\infty$–based attitude controller with anti-windup, which shows superior performance to a common PID-like controller. Particularly the robustness against input disturbances is considered, because main error sources in attitude control are aerodynamic torques and wind gusts.

2 Modelling

In various papers the quadrotor dynamics are derived, see [3], [6] or [5]. In this paper we are concerned with the results of our identification experiments in order to identify the dynamics that have an actual impact.

2.1 Quadrotor Dynamics

In figure 1, a schematic representation of a quadrotor is shown: Each motor produces a torque $\boldsymbol{\tau}$ with respect to the center of gravity. By individually varying

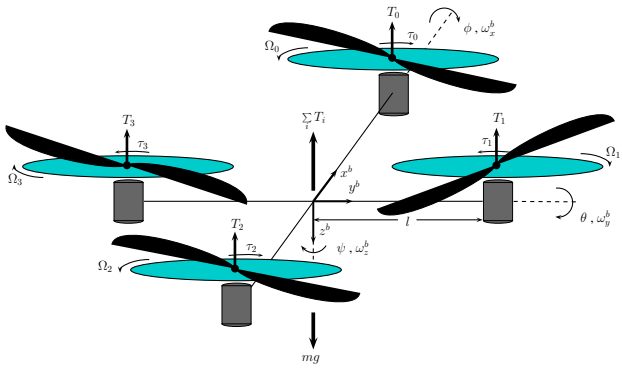

Figure 1. Quadrotor forces $\boldsymbol{T}$, torques $\boldsymbol{\tau}$, rotational velocities $\boldsymbol{\Omega}$, Euler–angles (ϕ, θ, ψ) and coordinate system

the produced thrust of the motors, the overall-torque will be non–zero, permitting the quadrotor to rotate about all three body-fixed axes with an angular velocity $\boldsymbol{\omega}$. If we assume a diagonal inertia matrix $\boldsymbol{J}$ (which is a quite good approximation, regarding the fact that the quadrotor is mechanically symmetric) and following the formalism of Newton-Euler, one gets the following model:

$$\begin{aligned}
\dot{\omega}_x^b &= \frac{J_{yy} - J_{zz}}{J_{xx}} \omega_y^b \omega_z^b + \frac{1}{J_{xx}} \tau_x \\
\dot{\omega}_y^b &= \frac{J_{zz} - J_{xx}}{J_{yy}} \omega_x^b \omega_z^b + \frac{1}{J_{yy}} \tau_y \\
\dot{\omega}_z^b &= \frac{J_{xx} - J_{yy}}{J_{zz}} \omega_x^b \omega_y^b + J_R \dot{\Omega}_r + \frac{1}{J_{zz}} \tau_z
\end{aligned} \tag{1}$$

with

$$\begin{aligned}
\Omega_R &= (\Omega_0 + \Omega_1 + \Omega_2 + \Omega_3) \\
\tau_x &= l(T_3 - T_1) \\
\tau_y &= l(T_0 - T_2) \\
\tau_z &= (\tau_0 + \tau_2 - \tau_3 - \tau_1)
\end{aligned} \tag{2}$$

The superscript b denotes the body frame. T_i is the thrust and τ_i the torque of the individual motors. The distance between the motors to the center of gravity is denoted as l, see figure 1.

2.2 Thrust and Torque

Motor thrusts T_i and torques τ_i are a direct result of the motors performing work on the air.

The input of the motor plant is a nondimensional number $b \in [0..1]$ which is sent via a digital interface to the motor controller, which actually performs the sensorless commutation for the brushless DC-motors. The output is the angular speed Ω. With the help of a simple experiment, one can identify the relation of Ω and b to be

$$\Omega(b) = a_0 \cdot b^{a_1} + a_2, \tag{3}$$

with scalar coefficients $a_0, a_1, a_2 \in \mathbb{R}$. The relation between motor speed and thrust/torque can be found by any introductory aerodynamic text to be

$$T = C_T \cdot \rho A R^2 \Omega^2 \tag{4}$$

$$Q = C_Q \cdot \rho A R^3 \Omega^2, \tag{5}$$

in which C_T and C_Q denotes the nondimensional thrust and torque coefficients, A the rotor disc area and R the rotor radius.

2.3 Motor Dynamics

We use brushless DC-motors with very low inductance. So the dynamics are approximated by a first-order ODE of the form

$$\dot{\Omega} = \kappa_1 \Omega + \kappa_2 V_{in}. \tag{6}$$

The coefficients κ_1 and κ_2 are motor specific. The motor dynamics are then modelled by the transfer-function

$$G_m = \frac{|p|}{s+p}. \tag{7}$$

Note that eq. (7) is normalized to 1, so it only covers the dynamics of the motor. Note also that $Q(\Omega)|_{\Omega_H} = Q(\Omega(b)|_{b_H})|_{\Omega(b_H)} = Q(\Omega(b_H)) + q\Gamma(b - b_H)$, where $q = 2C_Q \rho A R^3 \Omega_H$ is the linearization of eq. (5) around Ω_H and $\Gamma = a_0 a_1 b_H^{a_1 - 1}$ is the linearization of eq. (3) around b_H.

3 Model for controller design

Both quadrotor dynamics and force/torque generation are nonlinear, so we need to linearize if we want to use linear controller design techniques. We first have a look at quadrotor dynamics in eq. (1): As one can see, the nonlinear coupling terms only act, if the quadrotor rotates about at least two axis at a time. The moments of inertia for x and y are approximately the same, so the term for z cancels, while J_{zz} is slightly higher. Experiments show, that the nonlinear effects of the left over terms for x and y can be neglected in closed-loop operation, see [8]. Looking at the yaw-equation, one sees the additional linear term $J_r \dot{\Omega}$. This torque directly relates to the time derivative of angular momentum L

$$\dot{\boldsymbol{L}} = \boldsymbol{M} = J_r \dot{\boldsymbol{\Omega}}, \tag{8}$$

with J_r being the combined inertia of the rotors and motors. That means when the motors change their speed, the time derivative of angular momentum will be nonzero, causing a torque about the z-axis. Once the speed change of the motors has stopped, $\boldsymbol{L}$ will be constant again. This results in a very fast response on yaw with a fast decay–time, comparable to the D-part of a PID-controller. By neglecting the nonlinear coupling terms and defining $(\boldsymbol{\Phi}, \dot{\boldsymbol{\Phi}})^T$ with output $\boldsymbol{\Phi} = (\phi, \theta, \psi)^T$, we get the following transfer function:

$$\begin{pmatrix} \boldsymbol{\Phi} \\ \dot{\boldsymbol{\Phi}} \end{pmatrix} = \begin{pmatrix} \phi \\ \theta \\ \psi \\ \dot{\phi} \\ \dot{\theta} \\ \dot{\psi} \end{pmatrix} = \begin{pmatrix} \frac{1}{J_{xx}s^2} & 0 & 0 \\ 0 & \frac{1}{J_{yy}s^2} & 0 \\ 0 & 0 & \frac{(s+z)}{J_{zz}s^2} \\ \frac{1}{J_{xx}s} & 0 & 0 \\ 0 & \frac{1}{J_{yy}s} & 0 \\ 0 & 0 & \frac{(s+z)}{J_{zz}s} \end{pmatrix} \cdot \begin{pmatrix} \tau_x \\ \tau_y \\ \tau_z \end{pmatrix} \tag{9}$$

Now, let's have a look at the origin of the forces and torques: Equation (4) represents the equation of thrust in hover which depends quadratically on the angular rotor velocity Ω. By substituting eq. (3) in (4), (5) and linearizing about an operating point b_h one gets:

$$T = \frac{C_T}{C_Q R}\tilde{\Gamma} + \frac{C_T}{C_Q R} q\Gamma \cdot b + \cdots \text{ and} \tag{10}$$

$$Q = \quad \tilde{\Gamma} + \quad q\Gamma \cdot b + \cdots , \tag{11}$$

with

$$\tilde{\Gamma} = C_Q \rho A R^3 (a_0 b_H^{a_1} + a_2) \left[1 - 2(a_0 b_H^{a_1} + a_2) a_0 a_1 b_H\right]. \tag{12}$$

By neglecting higher order terms, (10) and (11) become linear equations of the form $y = mx + c$.

With that we can write our torques in form of $\boldsymbol{\tau} = (\tau_x, \tau_y, \tau_z)^T = \boldsymbol{K}\boldsymbol{b} + const.$

The overall model used for identification is then:

$$\begin{pmatrix} \boldsymbol{\Phi} \\ \dot{\boldsymbol{\Phi}} \end{pmatrix} = \begin{pmatrix} \frac{1}{J_{xx}s^2} & 0 & 0 \\ 0 & \frac{1}{J_{yy}s^2} & 0 \\ 0 & 0 & \frac{(s+z)}{J_{zz}s^2} \\ \frac{1}{J_{xx}s} & 0 & 0 \\ 0 & \frac{1}{J_{yy}s} & 0 \\ 0 & 0 & \frac{(s+z)}{J_{zz}s} \end{pmatrix} \cdot \begin{pmatrix} K_x \frac{|p_0|}{s+p_0} e^{-sT_d} \cdot b_x \\ K_y \frac{|p_0|}{s+p_0} e^{-sT_d} \cdot b_y \\ K_z \frac{\tilde{K}_z |p_1|}{s+p_1} e^{-sT_d} \cdot b_z \end{pmatrix} \tag{13}$$

Note that we introduced an additional factor $\tilde{K}_z$ and that the engine pole for yaw is different than for roll and pitch. This is a direct result of the identification procedure: While fixing the pole at the same value as roll/pitch, the optimization process needs more variance to converge to a reasonable solution in form of a additional zero and pole. These can then be approximated by changing the

fixed pole and gain, like denoted in eq. (13). A possible explanation is, that experiments for roll and pitch have been performed in a test rig, which only permits movement about one axis. In contrast, the experiment for yaw has been performed in free flight, which allows more vibration.

4 Grey–Box Parameter Identification

Due to unstable system dynamics of the quadrotor, the parameter identification has been performed in closed-loop. A Pseudorandom Binary Sequence (PRBS) γ of full length is used to excite the system. To improve the signal-to-noise ratio we averaged the experiments over ten periods, respectively. As stated before all three axes of the quadrotor have been identified separately. For that purpose we fixed the quadrotor in a test rig, allowing rotation only about one axis. The identification for the yaw–axis has been performed in free flight, though, because of the lack of an approriate test rig. Even though an operator is still required during free flight experiments for safety reasons, the operator can minimize possible noise introduced by reference steps, by limiting his commands to roll and pitch. Recall from eq. (1), that a reference step on roll/pitch influences yaw only through the nonlinear coupling term. Because of that it is also possible to average over several periods of γ, as stated above. The generic scheme of the identification process is depicted in figure 2. Note that the used PRBS-signal is persistently exciting of order $\gg 4$, which is sufficient for our purpose.

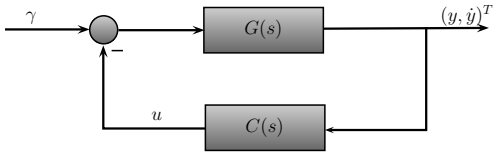

Figure 2. Indirect closed–loop identification setup

The controller $C(s)$ used during identification is a simple stabilizing, hand-tuned PD-controller with known parameters. Using equation (13), the identification signal γ, the controller C and output data $(y, \dot{y})^T$, we can use nonlinear optimization to estimate our parameter vector $\boldsymbol{\Delta}_{\phi,\theta} = (p, J, T_d)^T$ and $\boldsymbol{\Delta}_{\psi} = (p, z, J, T_d)^T$ respectively. Note that we excluded K from the parameter vector, because it can be calculated a–priori: The aerodynamic coefficients C_Q and C_T have been calculated using Blade Element Momentum Theory (BEMT), [9]. Note also, that you do not need this a–priori knowledge, even though you would not be able to distinguish between K and J in that case. See table 1 and 2 for results.

Figure 3 compares the simulation results of the identified models to a validation data set. For both, the simulation and the validation experiment, the same stabilizing controllers were used to close the unstable open–loop.

Table 1. Results of parameter estimation

	ϕ	θ	ψ
J	0.0181	0.0196	0.0273
p	-27.106	-26.963	-7.171
z	–	–	-2.434
T_d	0.024	0.028	0.016

Table 2. A-priori knowledge

l	$0.23m$
R	$0.127m$
C_T	0.0157
C_Q	0.0015
a_0	$701.2\frac{1}{s}$
a_1	0.8069
a_2	$-34.15\frac{1}{s}$
b_H	0.6

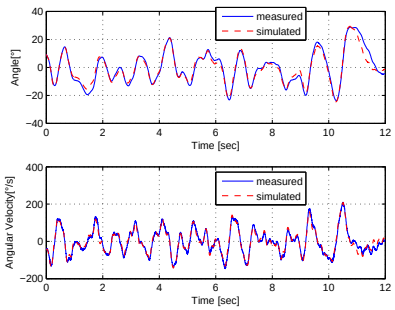

(a) pitch

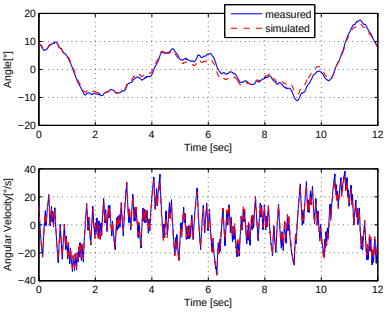

(b) yaw

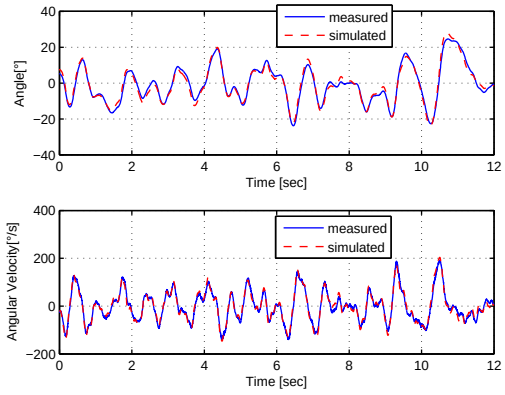

(c) roll

Figure 3. Simulation of the final linear models for a validation data set for the pitch (a), yaw(b) and roll(c) axis. Due to unstable system dynamics simulation has been performed in closed-loop with the same stabilizing controller as used for identification.

5 Controller Design

We have designed three separate attitude controllers using $\mathcal{H}_\infty$-loop-shaping with the derived models of the quadrotors rotational axes from section 4. Recall

that our models, which will be denoted as $G(s)$ respectively from now on, are single-input, multiple output (SIMO). Accordingly, our controllers $C(s)$ will be MISO. Our design goals are zero steady-state error, fast rise-time with little overshoot and good input-disturbance rejection.

The generalized plant used for the controller design is plotted in figure 4(a). To deal with input disturbances (e.g. wind gusts) we introduced an input d additionally to the reference input r. The prefilters V_d and $\mathbf{V_r}$ are scalar coefficients to weight between the channels with

$$\mathbf{V_r} = \begin{pmatrix} V_{r_1} & 0 \\ 0 & V_{r_2} \end{pmatrix}. \tag{14}$$

The shaping filters $W_K(s)$ and $\mathbf{W_S}(s)$ are first order transfer functions with

$$\mathbf{W_S}(s) = \begin{pmatrix} W_S(s) & 0 \\ 0 & 0 \end{pmatrix}. \tag{15}$$

The remaining filter $W_T(s)$ is only a static gain to reduce overshoot. The bandwidth of the controller has already been defined by $W_K(s)$ and $W_S(s)$.

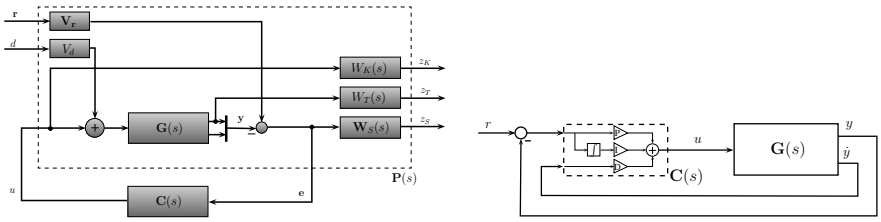

(a) Generalized plant for $\mathcal{H}_\infty$– controller design

(b) Structure of modified PID

Figure 4. (a) Generalized plant for $\mathcal{H}_\infty$– controller design, (b) Structure of the modified PID-controller.

For the evaluation of our controller performance, we have designed a modified PID controller, commonly used for quadrotor attitude control, see e.g. [10]. Its parameters are tuned by means of optimizing the simulated system response. Its generic structure is shown in figure 4(b). The main modification is the direct feedback of the time derivative $\dot{y}$ of the output y, because it can be measured directly, so there is no need for additional differentiation. Thus the D-part is just a static gain.

In figure 5 the results of a 10° reference step with the corresponding control inputs are plotted. It can be seen that both controllers have a rise time of $\approx 200ms$ with little overshoot, even though the PID-controllers have worse reference tracking. In figure 6 the results of an input disturbance of 10% of the maximum possible torque is shown. Here, our controller shows superior performance with a maximum displacement of only 4°, whereas the PID goes up to a

displacement of 15° and it takes about four seconds longer to compensate the disturbance.

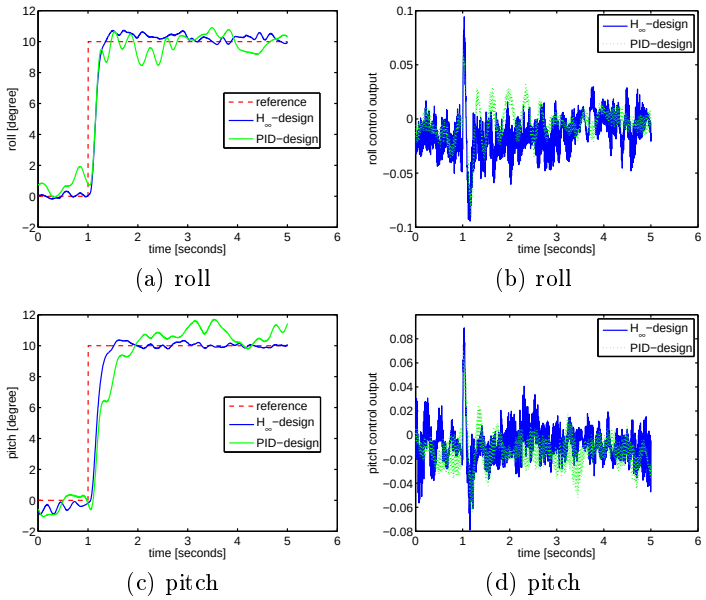

(a) roll (b) roll

(c) pitch (d) pitch

Figure 5. (left): Response to a 10° step for roll and pitch. (right): Corresponding control output

6 Anti-Windup Synthesis

This section deals with the design of an anti-windup compensator that accounts for input saturation due to actuator constraints. For this purpose, the existing linear $\mathcal{H}_\infty$ controller is augmented with an anti-windup compensation scheme which becomes active only when saturation occurs. The augmentation technique also prevents a re-design of the existing control algorithm while limiting degradation of the closed-loop performance during saturation periods. The idea of the anti-windup synthesis using Riccati equations is taken from [11].

6.1 Design Procedure

Figure 7 shows the generic anti-windup scheme, where $G(s)$ is the plant given in section 4 and $K(s)$ is the $\mathcal{H}_\infty$ controller described in section 5 designed to stabilize the nominal plant while fulfilling desired performance specifications. The anti-windup compensator is given as $\Theta(s)$ which only becomes active once the actuators are saturated. Note that the compensator $\Theta(s)$ has one input

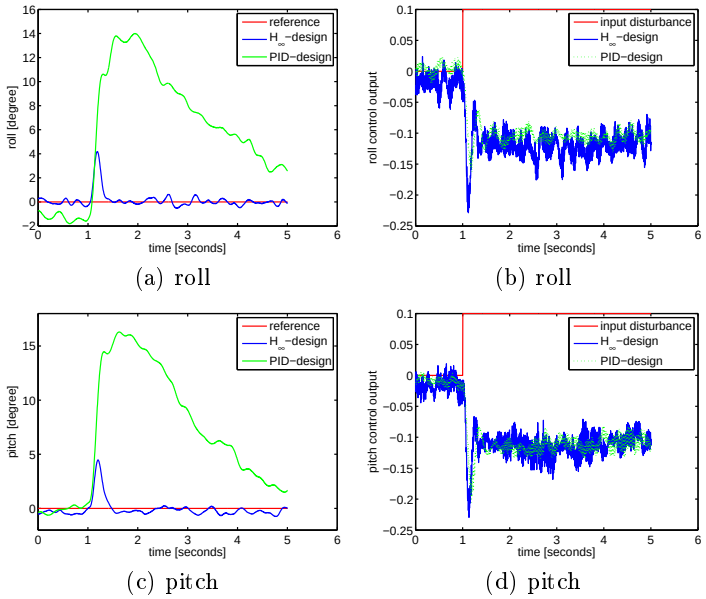

(a) roll (b) roll

(c) pitch (d) pitch

Figure 6. (left): Response to a input disturbance equivalent to 10% of maximum engine thrust for roll, pitch. (right): Correspondig control output

$\tilde{u} = u - u_\mathrm{m}$ and two outputs u_d and y_d which act on the controller output and the controller input, respectively. A parametrization of the anti-windup compensator

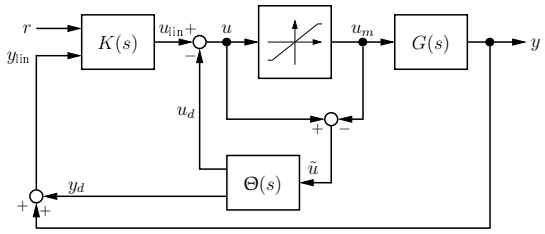

Figure 7. Generic anti-windup scheme

which is completely independent of the controller $K(s)$ is given in [12]. A state-space representation for the anti-windup compensator is given as

$$\Theta = \begin{bmatrix} \Theta_1 \\ \Theta_2 \end{bmatrix} \sim \begin{cases} \dot{x}_{aw} &= (A + BF)\, x_{aw} + B\tilde{u} \\ u_d &= F x_{aw} \\ y_d &= (C + DF)\, x_{aw} + D\tilde{u}, \end{cases} \tag{16}$$

where A, B, C, D are the state space matrices of the plant $G(s)$, F is a free parameter and $A + BF$ must be Hurwitz. The synthesis procedure is based on minimizing a scalar $\gamma > 0$ such that the induced 2-norm of the transfer function from the controller output u_{lin} to the compensator output y_d is smaller than a positive real scalar γ, or

$$\|\mathcal{T}_{y_d u_{\text{lin}}}\|_{i,2} \leq \gamma. \tag{17}$$

The details of the construction of the anti-windup compensator $\Theta(s)$ are given in [11], Theorem 1.

6.2 Experimental Results

Experimental validation of the anti-windup compensator was carried out with the help of a test rig, where a input disturbance of 30% of the maximal motor power was injected to the quadrotor robot. A comparison between the $\mathcal{H}_\infty-$ controller, described in section 5, with and without an anti-windup compensator was performed. Figure 8 shows the results of experiments in terms of the roll angle ϕ over time.

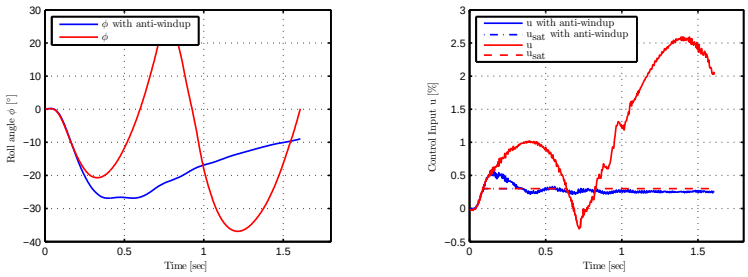

(a) Roll angle ϕ (b) Control input for ϕ

Figure 8. Roll angle ϕ and corresponding control input of an input disturbance rejection experiment

From figure 8(a) it can be observed that the anti-windup compensation scheme is able to stabilize the quadrotor robot despite the input disturbance and to bring the roll angle ϕ asymptotically to the origin, whereas without anti-windup compensator unstable behavior occurs.

In figure 8(b), it is shown how the anti-windup compensator influences the control input such that the linear region is reached after an actuator saturation event has occured. After recovery from saturation, the control input always stays close below the saturation boundary which also indicates good disturbance rejection properties.

7 Conclusion

In this paper we have presented our results for linear model identification of the quadrotors rotational axes under real, non-ideal conditions. The derived models include a first-order transfer function for the motors, while aerodynamic coefficients have been estimated using BEMT. The experimental results show a very good correlation with real data, which confirms the proposed Grey–Box approach. In addition to the model identification, we designed robust $\mathcal{H}_\infty$ attitude controllers. They have superior performance to commonly used modified PID controllers, particularly with regard to input disturbance rejections, but also to rise-time and reference tracking. Just to deal with input saturations, we augmented the attitude controllers with an anti-windup compensator based on Riccati-equations. This integrated anti-windup compensator leads to a further improvement of the performance, e.g. under harsh environmental conditions.
In the future we will account for nonlinear aerodynamic effects to especially optimize the control during forward flight.

References

1. Michael, N., Mellinger, D., Lindsey, Q., Kumar, V.: The GRASP Multiple Micro-UAV Testbed. Robotics & Automation Magazine, IEEE **17**(3) (2010) 56–65
2. Lupashin, S., Schollig, A., Hehn, M., D'Andrea, R.: The Flying Machine Arena as of 2010. In: Robotics and Automation (ICRA), 2011 IEEE International Conference on, IEEE (2011) 2970–2971
3. Hoffmann, G., Huang, H., Waslander, S., Tomlin, C.: Quadrotor Helicopter Flight Dynamics and Control: Theory and Experiment. In: Proceedings of the AIAA Guidance, Navigation, and Control Conference. Volume 4. (2007) 44
4. Witt, J., Annighöfer, B., Falkenberg, O., Weltin, U.: Design of a High Performance Quad-Rotor Robot Based on a Layered Real-Time System Architecture. Intelligent Robotics and Applications (2011) 312–323
5. Bouabdallah, S.: Design and Control of Quadrotors with Application to Autonomous Flying. Ecole Polytechnique Federale de Lausanne (2007)
6. Beard, R.: Quadrotor Dynamics and Control. (2008)
7. Fay, G.: Derivation of the Aerodynamic Forces for the Mesicopter. (2001)
8. Falkenberg, O.: Robuste Lageregelung und GPS/INS-Integration eines autonomen Quadrokopters. Hamburg University of Technology (2010)
9. Leishman, J.: Principles of Helicopter Aerodynamics. Cambridge Univ Pr (2006)
10. Tayebi, A., McGilvray, S.: Attitude Stabilization of a VTOL Quadrotor Aircraft. Control Systems Technology, IEEE Transactions on **14**(3) (may 2006) 562 – 571
11. Sofrony, J., Turner, M., Postlethwaite, I.: Anti-Windup Synthesis Using Riccati Equations. International Journal of Control **80**(1) (2007) 112–128
12. Weston, P., Postlethwaite, I.: Linear Conditioning for Systems Containing Saturating Actuators. Automatica **36**(9) (2000) 1347–1354
13. Pilz, U., Gropengießer, W., Walder, F., Witt, J., Werner, H.: Quadrocopter Localization Using RTK-GPS and Vision-Based Trajectory Tracking. Intelligent Robotics and Applications (2011) 12–21
14. Ljung, L.: System Identification: Theory for the User. Pearson Education (1998)
15. Witt, J.: Approximate Model Predictive Control for Nonlinear Multivariable Systems. In: Model Predictive Control, InTech (2010) 141–166